Journal of Solid State Chemistry **149,** 242–251 (2000)
doi:10.1006/jssc.1999.8523, available online at http://www.idealibrary.com on IDEAL®

Synthesis and Structures of Ternary Chalcogenides of Aluminum and Gallium with Stacking Faults: KMQ_2 (M = Al, Ga; Q = Se, Te)

Joonyeong Kim and Timothy Hughbanks[1]

Department of Chemistry, Texas A&M University, P.O. Box 30012, College Station, Texas 77842-3012

Received June 23, 1999; in revised form September 15, 1999; accepted October 1, 1999

The synthesis and crystal structures of new ternary chalcogenides of aluminum and gallium, KMQ_2 (M = Al, Ga; Q = Se, Te) are reported. These compounds were synthesized by solid-state reaction at 800°C in Nb containers. The single-crystal structures of $KMTe_2$ (M = Al, Ga) have been determined; $KAlTe_2$, a = 11.808(2) Å, b = 11.812(2) Å, c = 16.456(3) Å, β = 100.32(3)°, $C2/c$ (No. 15, Z = 16); $KGaTe_2$, a = 11.768(3) Å, b = 11.775(3) Å, c = 16.503(4) Å, β = 100.36(2)°, $C2/c$ (No. 15, Z = 16). The fundamental building blocks of the title compounds are adamantane-like M_4Q_{10} ($M_4Q_{10} = M_4Q_4Q_{12/2}$) supertetrahedra consisting of four MQ_4 (M = Al, Ga; Q = Se, Te) tetrahedra. These supertetrahedra form two-dimensional $^2_\infty[M_4Q_6Q_{4/2} = MQ_2]^-$ layers by sharing terminal chalcogen atoms with adjacent supertetrahedra. These layers form a stack up to the c axis with each layer rotated by 90° relative to its neighbors. Potassium cations are located inside trigonal prisms formed by six chalcogen atoms. Stacking faults up the c^* axis are evidenced by streaks in oscillation photographs. Only half of the data set is affected by this type of faulting. We demonstrate both analytically and by use of the DIFFaX program that our structural model for the faulting is consistent with the observed streaking patterns. © 2000 Academic Press

Key Words: **ternary chalcogenides of aluminum and gallium; solid-state synthesis; crystal structures; layered compounds; stacking fault; OD structure; DIFFaX program.**

INTRODUCTION

Planar faulting is a widespread phenomenon in real crystals and has been of interest to many physicists and crystallographers (1–11). Planar faulting typically occurs in layered structures that lack order in the layer stacking sequence because there are two or more geometrically and energetically comparable ways in which neighboring layers may be placed with respect to one another. Accordingly, the diffracted intensity from a large sample of faulted crystals is the weighted, incoherent sum of the diffraction patterns arising from each occurring crystallite orientation and defect arrangement. Sometimes, diffuse reflections and streaks, as well as sharp reflections, are observed in the diffraction patterns of this class of crystals, especially order–disorder (OD) type crystals (2, 3, 12, 13). The diffraction patterns for such crystals may show systematic absences that do not corresponding to any of the 230 crystallographic space groups possible for three-dimensionally periodic structures. Many methods of calculating diffraction intensities for crystals with planar faults have been devised, including the Hendricks–Teller matrix formulation (14), Wilson's difference equation method (15, 16), the summed series formula of Cowley (7–9), Michaliski's recurrence relations between average phase factors (10, 11), and Treacy's general recursion method (1).

Our investigation of crystals with planar faults was initiated by the discovery of new ternary compounds KMQ_2 (M = Al, Ga; Q = Se, Te). Oscillation photographs of crystals of these compounds exhibit sharp peaks as well as streaks and diffuse reflections which are characteristic of crystals with stacking faults (Fig. 1). These compounds were synthesized during our exploration of K–M–Q (M = Al, Ga; Q = Se, Te) ternary chalcogenides of group 13 as a part of our effort to synthesize new layered polar compounds that are isostructural with $AMnQ_2$ (A = Li, Na; Q = Se, Te) (17–20).

Early investigations of the K–M–Q (M = Al, Ga; Q = Se, Te) systems by Weiss and Eisenmann yielded a number of compounds, K_5GaSe_4, K_3MQ_3 (M = Al, Ga; Q = Se, Te), $KAlTe_2$, and KMQ_2 (Q = Se for M = Al; Q = Se, Te for M = Ga) (21–26). Discrete $[GaSe_4]^{5-}$ and $[MQ_3 = M_2Q_4Q_{4/2}]^{3-}$ dimers formed by fusion of two MQ_4 tetrahedra are found in the first and second class of compounds, respectively. The third possesses one-dimensional $^1_\infty[AlTe_2 = AlTe_{4/2}]^-$ chains. The structure of the fourth class of compounds was not determined, but they belong to a triclinic system with $a = b$ and $\alpha = \beta = \gamma \cong 90°$ (21).

In this paper, the synthesis and characterization of ternary compounds KMQ_2 (M = Al, Ga; Q = Se, Te) and the planar faults exhibited by this class of compounds will be

[1]To whom correspondence should be addressed. Fax: (409) 847-8860. E-mail: trh@mail.chem.tamu.edu.

0022-4596/00 $35.00

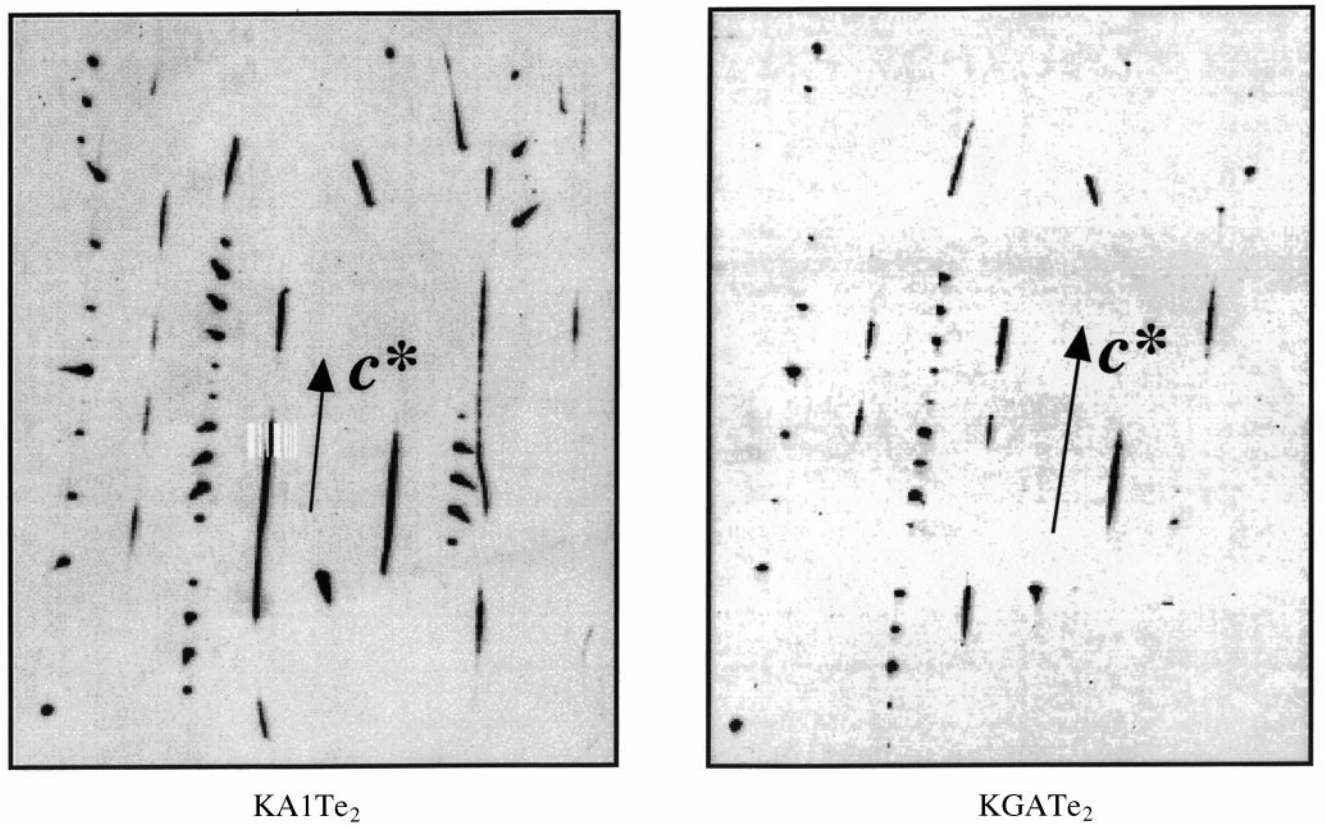

FIG. 1. Oscillation photographs of $KAlTe_2$ and $KGaTe_2$.

discussed. Structure factor calculations based on Cowley's modified summed series formula will be introduced to rationalize the nature of stacking faults and their influence on the diffraction intensities (7–9). Finally, we will present simulated diffraction patterns (generated with the program DIFFaX) calculated by assuming the presence of the stacking faults described in this paper (27).

EXPERIMENTAL SECTION

Materials and Instrumentation

The ternary and binary compounds described herein are sensitive to both moisture and oxygen, experimental operations were carried out under a nitrogen atmosphere. Elemental starting materials Al (99.95%, Aldrich), Ga (99.9%, Johnson Matthey), Te (99.997%, Aldrich), Se (99.999%, Aldrich), and K (99.9%, Aldrich) were used as received. K_2Se and K_2Te were synthesized in liquid NH_3, and binary metal chalcogenides M_2Q_3 (M = Al, Ga; Q = Se, Te) were prepared in silica tubes by methods described in the literature (28–33). The purity of these starting binary chalcogenides was confirmed by examination of Guinier X-ray powder patterns.

Atomic absorption (AA) measurements were performed on a Varian SpectrAA 250 Plus instrument after the dissolution of the products in 20% (w/w) nitric acid. Standard solutions for AA measurements were purchased from Aldrich. For each element, measurements of at least three standard solutions were taken with different concentrations to obtain a linear calibration plot.

Wavelength-dispersive X-ray spectrometric (WDS) analyses were performed using a Cameca SX 50 electron microprobe equipped with four WDS spectrometers. Each spectrometer contained an X-ray diffraction crystal as a monochromator and a gas-flow proportional ionization detector. For each element analyzed, a well-characterized compound or pure element was used as a standard. Crystals of ternary compounds were collected and mounted on the top of sample holders with double-sided carbon tape. For each compound, measurements were performed at least three times for independent crystals, and analyses were processed through the Cameca PAP full-quantitative matrix correction program (34).

Synthesis

All ternary chalcogenides, KMQ_2 (M = Al, Ga; M = Se, Te) were synthesized by mixing either elemental starting materials, K, Al (or Ga), and Se (or Te), or binaries, K_2Q (Q = Se, Te) and M_2Q_3 (M = Al, Ga; Q = Se, Te), in

a stoichiometric ratio by the use of Nb tubes that were in turn sealed in evacuated ($\sim 10^{-4}$ Torr) silica tubes. Excess chalcogen (3–5%) was added in each case. In the case of $KMSe_2$ (M = Al, Ga), the temperature was uniformly raised to 250°C over 12 h, held at that temperature for 2 days, raised to 800°C over the next 48 h, held at that temperature for 10 days, then cooled to 350°C at a rate of 2°C/h, and finally quenched to room temperature. For ternary tellurides, $KMTe_2$ (M = Al, Ga), the temperature of the reaction vessel was uniformly raised to 500°C over 2 days, maintained at 500°C for 2 days, uniformly increased to 800°C for 2 days, and then maintained at that temperature for 10 days. The vessel was then cooled to 350°C at a rate of 2°C/h and finally quenched to room temperature. Single crystals suitable for the X-ray studies and microprobe analysis were found within each reaction product. SEM images of $KMTe_2$ (M = Al, Ga) are shown in Fig. 2.

Microprobe analysis on selected crystals from each compound showed approximate compositions $K_{1.20(2)}Al_{1.01(2)}Se_2$, $K_{0.90(1)}Al_{0.92(3)}Te_2$, $K_{0.94(2)}Ga_{1.00(2)}Se_2$, and $K_{0.94(1)}Ga_{1.00(3)}Te_2$ for $KAlSe_2$, $KAlTe_2$, $KGaSe_2$, and $KGaTe_2$, respectively. No other elements heavier than Na, including Nb, were found. For the same compounds, AA measurements gave the compositions $K_{0.98(4)}Al_{0.95(3)}Se_2$, $K_{0.89(2)}Al_{1.03(5)}Te_2$, $K_{1.05(3)}Ga_{1.06(3)}Se_2$, and $K_{0.99(2)}Ga_{1.07(3)}Te_2$.

X-Ray Crystallography

X-ray diffraction data for $KAlTe_2$ and $KGaTe_2$ were collected using a Siemens R3m/V diffractometer with graphite monochromated Mo$K\alpha$ radiation ($\lambda = 0.71073$ Å) at 20°C. For $KGaTe_2$, another data set was collected independently using a Siemens (Bruker) SMART CCD (charge-coupled device)-equipped diffractometer at 20°C, and this data set was used to refine the final structure. The cell parameters of $KGaTe_2$ obtained using both systems were nearly identical. Structure refinements were based on F^2 with the use of the SHELX-93 package of programs (35).

A white transparent crystal of $KAlTe_2$ having approximate dimensions $0.10 \times 0.30 \times 0.60$ mm and an orange-yellow transparent crystal of $KGaTe_2$ having approximate dimensions $0.10 \times 0.30 \times 0.50$ mm were mounted in each glass capillary. Initial cell constants and an orientation matrix for each compound were obtained from a least-squares refinement using the setting angles from at least 25 centered reflections from the rotational photograph. Axial photographs indicated that the correct a and b axes are two times longer than those obtained from initial rotational photographs. Subsequently, corrected cell parameters were refined by centering on 36 reflections in the range $15^\circ \leq 2\theta \leq 45^\circ$. Three check reflections were monitored every 97 reflections throughout the data collection process in each compound. The data were corrected for absorption using the ψ-scan technique based on at least five reflections. A quadrant of the data ($+h$, $+k$, $\pm l$) was collected by use of θ–2θ scans with $2\theta < 51^\circ$ for $KAlTe_2$ and with $2\theta < 55^\circ$ for $KGaTe_2$. Careful inspection of the data reveals that half of each data set ($2h + 1$, $2k + 1$, l) was affected by disorder, and such data were not used in the refinement process for either compound. The stacking fault model discussed below

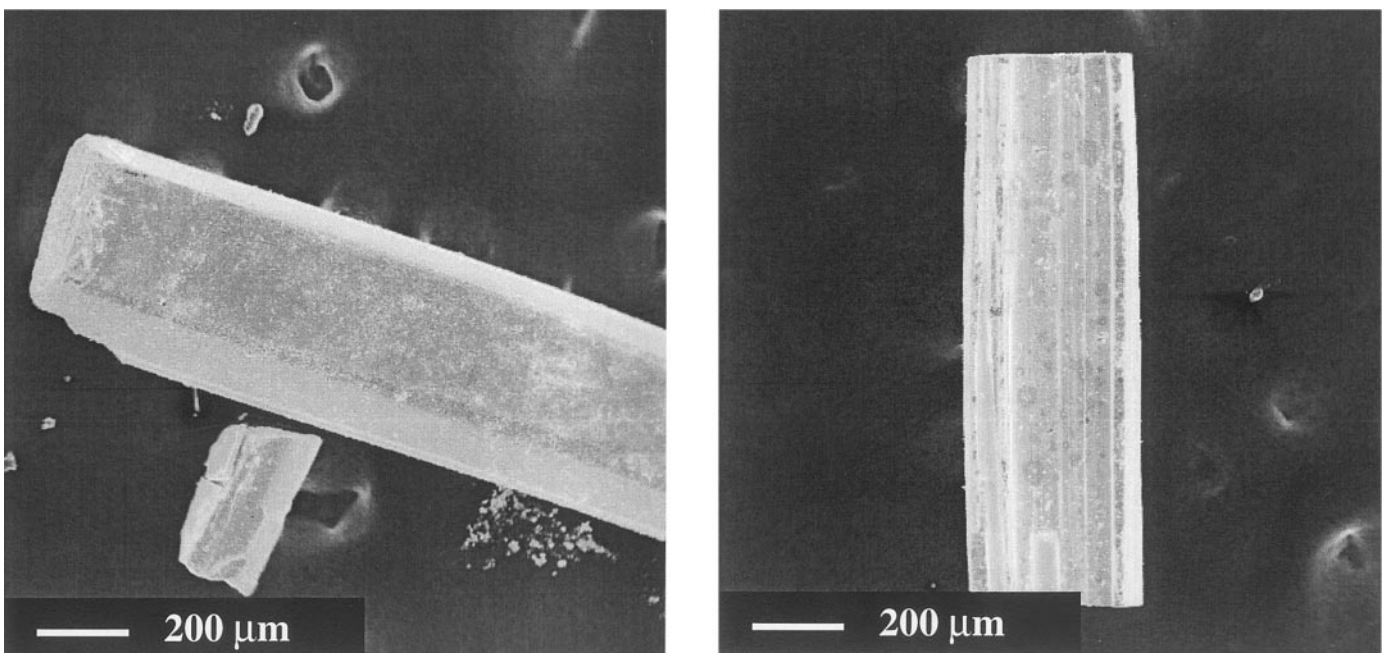

FIG. 2. SEM images of $KAlTe_2$ (left) and $KGaTe_2$ (right).

is offered as the explanation for the diffuse scattering associated with these reflections. Systematic absences, Guinier X-ray diffraction data, and elemental analysis suggested that ternary compounds, $KMTe_2$ (M = Al, Ga), are isostructural with the known phase $TlGaSe_2$, which had been refined in the space group Cc (No. 9) (36). We worked under the assumption that $TlGaSe_2$ properly belongs to the space group $C2/c$ (No. 15). These two space groups (Cc and $C2/c$) are indistinguishable by systematic absences. The new atomic positions for $TlGaSe_2$ comparable with $C2/c$ were generated by translations (along the a and c axes) and reflections (with respect to new origin in the $C2/c$ space group) of the original coordinates based on the Cc space group. These new coordinates contain several equivalent positions related by the twofold symmetric operation in $C2/c$. The $C2/c$ compatible atomic positions so derived for $TlGaSe_2$ were used to begin refinement of both $KAlTe_2$ and $KGaTe_2$. The data set obtained from the CCD diffractometer was used for the refinement of $KGaTe_2$. Final anisotropic refinement gave 2.41 and 5.21% for $KAlTe_2$ and 4.59 and 10.05% for $KGaTe_2$ for final $R(F)$ and $wR_2(F^2)$ with $I > 2\sigma(I)$, respectively. For $KGaTe_2$, a structure refinement using the data set collected using a Siemens R3m/V diffractometer gave atomic coordinates and residuals (R-values) nearly identical to those obtained with the CCD data set.

A summary of crystal and data collection parameters of $KAlTe_2$ and $KGaTe_2$ are listed in Table 1, final atomic coordinates are shown in Table 2, and the anisotropic thermal parameters are given in Table 3. Preliminary X-ray studies and elemental analyses revealed that ternary selenides $KMSe_2$ (M = Al, Ga) are isostructural with their telluride analogs. Refined cell parameters are $a = 10.885(6)$ Å, $b = 10.884(5)$ Å, $c = 15.382(7)$ Å, $\beta = 100.19(2)^\circ$ for $KAlSe_2$ and $a = 10.945(4)$ Å, $b = 10.947(3)$ Å, $c = 15.314(6)$ Å, $\beta = 100.22(5)^\circ$ for $KGaSe_2$.

TABLE 1
Crystallographic Data for $KAlTe_2$ and $KGaTe_2$

Empirical formula:	$KAlTe_2$	$KGaTe_2$[a]
Crystal shape, color	plate, white	plate, red-orange
Crystal size (mm)	$0.10 \times 0.30 \times 0.60$	$0.10 \times 0.30 \times 0.50$
Space group, Z	$C2/c$ (No. 15), 16	$C2/c$ (No. 15), 16
a (Å)	11.808(2)	11.768(3)
b (Å)	11.812(2)	11.775(3)
c (Å)	16.465(3)	16.503(4)
β (°)	100.32(3)	100.36(2)
V (Å^3)	2259.3(7)	2249.5(9)
Formula weight	321.28	364.02
T (°C)	20	20
λ (Å)	0.71073	0.71073
ρ_{calcd} (g/cm^3)	3.778	4.299
μ (mm^{-1})	11.047	15.627
$2\theta_{max}$ (°)	51.00	55.10
h, k, l range	14, 14, ±19	−14, −14, ±21
$F(000)$	2176	2464
No. of collected reflections	4631	5719
No. of unique reflections[b]	1048	1303
No. of reflections ($I \geq 2\sigma(I)$)[c]	487	549
R_{int} (%)	1.85	3.59
Restraints/parameters	0/75	0/75
Goodness of fit	1.062	1.052
R_1[d], wR_2[e] (%)	2.41, 5.21	4.59, 10.05
x and y in wR_2[e]	0.032, 0.005	0.055, 77.233
Max., min. $\Delta\rho$ (eÅ^{-3})	0.489, −0.464	1.290, −1.260

[a] Data for $KGaTe_2$ were collected using a Bruker CCD-equipped diffractometer.

[b] Only ($2h$, $2k$, l) reflections were used in the refinements.

[c] Only ($2h$, $2k$, l) reflections were used in the computation of R_1 and wR_2 (%).

[d] $R_1(F) = \sum(||F_o| - |F_c||)/\sum(|F_o|)$.

[e] $wR_2(F^2) = [\sum|w(F_o^2 - F_c^2)^2|/\sum|w(F_o^2)^2|]^{1/2}$, $w = 1/[\sigma^2(F_o^2) + (xP)^2 + yP]$, where $P = (\max(F_o^2, 0) + 2F_c^2)/3$.

DISCUSSION

Structure

A (110) projection of the $KGaTe_2$ structure is shown in Fig. 3, and selected interatomic distances and angles of both $KMTe_2$ (M = Al, Ga) compounds are listed in Table 4. Fundamental building blocks of KMQ_2 (M = Al, Ga; Q = Se, Te) are M_4Q_{10} ($=(MQQ_{3/2})_4$) supertetrahedra. These supertetrahedra are formed by condensation of four MQ_4 tetrahedra (see Fig. 4). The MTe_4 (M = Al, Ga) tetrahedra in $KAlTe_2$ and $KGaTe_2$ are slightly distorted; Al–Te distances in $KAlTe_2$ range from 2.58(2) to 2.63(1) Å and Ga–Te distances in $KGaTe_2$ from 2.45(4) to 2.62(1) Å. The Te–Al–Te angles are between 105.4(4) and 113.0(6)° for $KAlTe_2$, and the Te–Ga–Te angles are in the range between 105.3(2) and 111.6(1)° for $KGaTe_2$. Two-dimensional $^2_\infty[(M_4Q_6)Q_{4/2} = MQ_2]^-$ layers are formed by fusion of supertetrahedra, M_4Q_{10}, sharing four corners with each other. As a result, the superlayers in KMQ_2 (M = Al, Ga; Q = Se, Te) can be considered as expanded analogs of those observed in $AMnQ_2$ (A = K, Rb, Cs; Q = Se, Te), which have layers formed by fusion of simple MnQ_4 tetrahedra (18, 19).

Adjacent layers are turned 90° with respect to each other and stacked up the c axis such that the layer ridges run parallel to the valleys in neighboring layers. K^+ ions sit within trigonal prisms formed by four Te atoms from the same layer and two Te atoms from the adjacent layer (see Figs. 4 and 5). K–Te contacts range from 3.56(1) and 3.61(2) Å in $KAlTe_2$ and from 3.49(2) and 3.82(5) Å in $KGaTe_2$. The shortest contacts between potassium atoms are 4.17(2) and 4.11(3) Å for $KAlTe_2$ and $KGaTe_2$, respectively.

Stacking Faults and Structure Factor Calculation

Our discussion will focus on $KGaTe_2$, but all the title compounds exhibit the stacking faults we will discuss.

TABLE 2
Atomic Coordinates and Equivalent Isotropic Displacement Parameters

Atom	Position	x	y	z	U_{eq}[a] (Å$^2 \times 10^3$)
			$KAlTe_2$		
Te1	4*e*	0.0	0.571(2)	1/4	20(3)
Te2	4*e*	0.0	0.054(2)	1/4	21(3)
Te3	8*f*	0.2037(3)	0.0624(3)	0.0635(2)	34(1)
Te4	8*f*	0.260(2)	0.3124(2)	0.248(2)	21(2)
Te5	8*f*	0.0468(4)	0.3125(3)	0.4356(2)	36(1)
Al1	8*f*	0.6029(9)	0.686(1)	0.1608(5)	12(3)
Al2	8*f*	0.147(1)	0.440(1)	0.3380(6)	24(3)
K1	8*f*	0.467(1)	0.3132(9)	0.1135(6)	45(3)
K2	8*f*	0.286(1)	0.061(1)	0.3876(6)	49(3)
			$KGaTe_2$		
Te1	4*e*	0.0	0.566(2)	1/4	45(4)
Te2	4*e*	0.0	0.059(1)	1/4	22(2)
Te3	8*f*	0.2034(4)	0.0624(4)	0.0649(2)	42(1)
Te4	8*f*	0.242(5)	0.3128(3)	0.248(3)	28(4)
Te5	8*f*	0.0457(4)	0.3127(4)	0.4354(3)	46(1)
Ga1	8*f*	0.6026(5)	0.6879(6)	0.1620(4)	20(1)
Ga2	8*f*	0.1462(5)	0.4372(6)	0.3373(4)	21(1)
K1	8*f*	0.464(1)	0.316(2)	0.1092(9)	54(5)
K2	8*f*	0.284(1)	0.060(2)	0.386(1)	47(4)

[a]Equivalent isotropic U defined as one-third of the trace of the orthogonalized U_{ij} tensor.

TABLE 3
Anisotropic Thermal Parameters (Å$^2 \times 10^3$) for $KAlTe_2$ and $KAlTe_2$

Atom	U_{11}	U_{22}	U_{33}	U_{12}	U_{13}	U_{23}
			$KAlTe_2$			
Te1	20(5)	11(6)	27(3)	0	3(3)	0
Te2	24(5)	10(6)	32(4)	0	9(3)	0
Te3	38(2)	44(2)	18(1)	33(2)	1(1)	3(1)
Te4	8(5)	24(1)	31(2)	− 1(2)	8(3)	− 5(3)
Te5	47(2)	44(2)	16(1)	− 27(2)	5(1)	3(1)
Al1	12(6)	19(6)	6(4)	1(5)	3(4)	− 5(4)
Al2	23(7)	13(6)	35(7)	− 8(5)	6(5)	− 6(5)
K1	48(7)	47(7)	38(6)	29(5)	3(5)	− 14(5)
K2	59(7)	67(8)	21(5)	− 28(6)	10(4)	− 18(5)
			$KGaTe_2$			
Te1	18(5)	44(7)	67(6)	0	− 7(3)	0
Te2	33(6)	19(3)	18(3)	0	15(3)	0
Te3	49(2)	56(3)	17(2)	40(3)	1(2)	3(2)
Te4	20(12)	25(2)	39(5)	1(2)	5(6)	6(4)
Te5	60(3)	57(3)	19(2)	− 44(3)	6(2)	2(2)
Ga1	15(2)	24(3)	21(2)	4(3)	4(2)	3(2)
Ga2	21(3)	17(3)	24(2)	− 4(3)	4(2)	3(2)
K1	75(9)	64(9)	23(6)	40(7)	9(6)	− 14(6)
K2	35(6)	61(9)	44(7)	− 25(6)	4(5)	− 16(6)

Orange HgI_2 consists of same type of two-dimensional $^2_\infty[(Hg_4I_6)I_{4/2} = HgI_2]$ layers formed by fusion of Hg_4I_{10} supertetrahedra and exhibits stacking faults due to the existence of two stacking possibilities in each layer (13). Accordingly, part of our descriptions of stacking faults in $KGaTe_2$ were adopted from the HgI_2 model. The layers in $KGaTe_2$ possess grooves that run parallel to the [110] direction on one side of a layer and identical grooves that run parallel to the $[1\bar{1}0]$ direction on the other side (see Fig. 5). Since these crevices interdigitate to some extent when the layers stack, a stacking pattern is adopted wherein alternant layers are rotated by 90° around the stacking axis with respect to their neighbors. We will refer to layers in which the top grooves (viewed looking down the stacking axis) run parallel to [110] as "A" layers and those in which the top grooves run parallel to $[1\bar{1}0]$ as "B" layers (see Fig. 5). The ideal structure of a $KGaTe_2$ crystal can be viewed as an infinite alternating stacking of two types of layers, A and B, from the bottom to the top (see Fig. 5). All layers propagate parallel to the *ab* plane and the stacking direction is along the c^*.

Stacking faults occur in $KGaTe_2$ because there are two stacking possibilities for placing any given layer over its neighbor. Each layer can be located in the ideal position (i.e., where it sits in the ordered structure discussed above) or it can be shifted by either $0.25(\mathbf{a} - \mathbf{b})$ or $0.25(\mathbf{a} + \mathbf{b})$ relative to the ideal position (Fig. 5). The potassium ion coordination environments are nearly identical (geometrically and energetically) when the layers stack in the ideal or faulted position.

We now outline the method by which stacking faults can be understood insofar as they affect diffraction intensities. Our discussion follows the general discussion of the summed series formula of Cowley (7–9). The total structure factor (F_T) is the sum of structure factors contributed from individual terms,

$$F_T(hkl) = \sum_i F_i = F_0 + F_1 + F_2 + \cdots + F_N, \qquad [1]$$

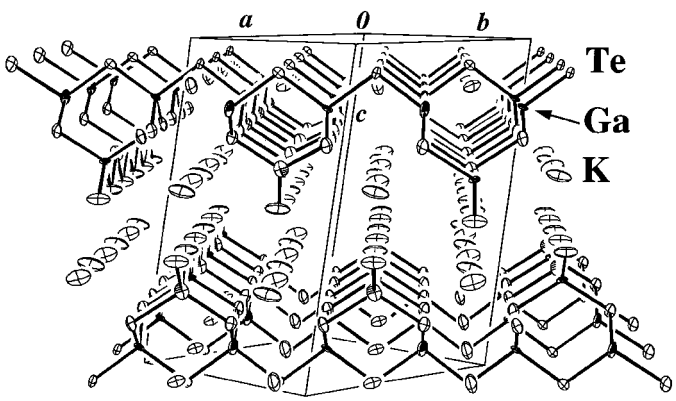

FIG. 3. Thermal ellipsoid plot (70% probability) of $KGaTe_2$.

TABLE 4
Important Interatomic Distances (Å) and Bond Angles (°) for $KAlTe_2$ and $KGaTe_2$

$KAlTe_2$		$KGaTe_2$	
Al1–Te2	2.59(2)	Ga1–Te2	2.55(1)
Al1–Te3	2.61(1)	Ga1–Te3	2.616(8)
Al1–Te4	2.60(2)	Ga1–Te4	2.45(4)
Al1–Te5	2.62(1)	Ga1–Te5	2.604(7)
Al2–Te1	2.58(2)	Ga2–Te1	2.54(1)
Al2–Te3	2.61(1)	Ga2–Te3	2.623(7)
Al2–Te4	2.63(2)	Ga2–Te4	2.49(4)
Al2–Te5	2.63(1)	Ga2–Te5	2.618(8)
K1–Te1	3.61(2)	K1–Te1	3.73(2)
K1–Te2	3.61(2)	K1–Te2	3.67(2)
K1–Te3	3.55(1)	K1–Te3	3.49(1)
K1–Te5	3.56(1)	K1–Te5	3.53(2)
K1–Te4	3.59(2)	K1–Te4	3.82(5)
	3.60(3)		3.77(5)
K2–Te1	3.69(1)	K2–Te1	3.68(1)
K2–Te2	3.71(1)	K2–Te2	3.68(1)
K2–Te3	3.53(1)	K2–Te3	3.56(2)
K2–Te5	3.55(1)	K2–Te5	3.58(2)
K2–Te4	3.67(2)	K2–Te4	3.63(3)
	3.73(2)		3.73(3)
K1–K2	4.17(2)	K1–K2	4.11(2)
	4.18(2)		4.22(3)
$KAlTe_2$		$KGaTe_2$	
Te2–Al1–Te3	108.9(7)	Te2–Ga1–Te3	109.1(3)
Te2–Al1–Te4	113.0(6)	Te2–Ga1–Te4	111.4(1)
Te2–Al1–Te5	110.6(5)	Te2–Ga1–Te5	110.7(3)
Te3–Al1–Te4	107.7(6)	Te3–Ga1–Te4	111.2(1)
Te3–Al1–Te5	106.2(3)	Te3–Ga1–Te5	105.6(2)
Te4–Al1–Te5	110.2(6)	Te4–Ga1–Te5	108.8(8)
Te1–Al2–Te3	109.1(7)	Te1–Ga2–Te3	109.1(4)
Te1–Al2–Te4	112.8(7)	Te1–Ga2–Te4	110.3(1)
Te1–Al2–Te5	110.7(5)	Te1–Ga2–Te5	110.5(3)
Te3–Al2–Te4	108.4(7)	Te3–Ga2–Te4	111.6(1)
Te3–Al2–Te5	105.4(4)	Te3–Ga2–Te5	105.3(2)
Te4–Al2–Te5	110.2(6)	Te4–Ga2–Te5	110.2(6)

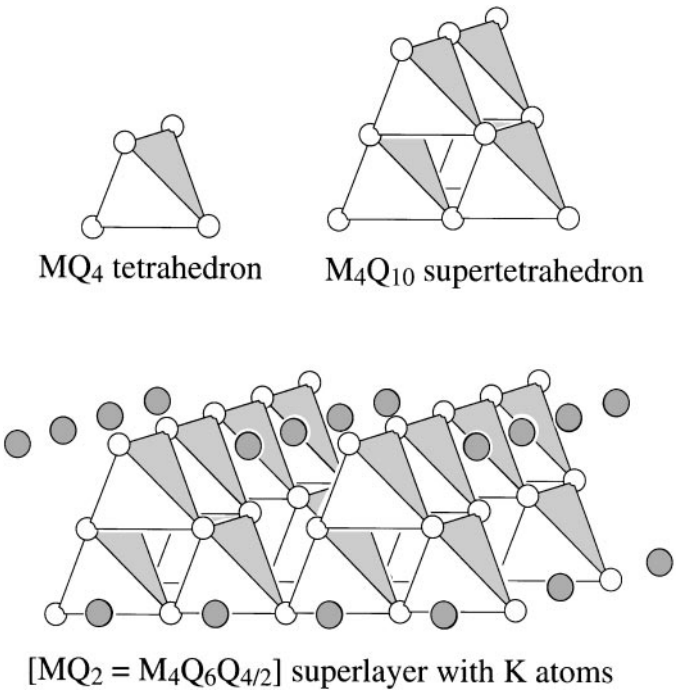

FIG. 4. Polyhedral representation of fundamental building blocks in KMQ_2 (M = Al, Ga; Q = Se, Te).

where F_i denotes the contributions to F_T that are due to the interference effects involving interatomic displacements for pairs of atoms, one of which lies in a given layer and the second of which lies in the ith nearest neighbor layer. To discuss F_i, several symbols need to be defined: g_A (g_B) is the probability that the bottom is layer A (B), so $g_A + g_B = 1$; α_{AB} (α_{BA}) is the probability that a stacking fault occurs for the B (A) layer, which is stacked after layer A (B); $\mathbf{r}_{AB}$ ($\mathbf{r}_{BA}$) is the fault vector by which the B (A) layer is shifted in the ab plane relative to the position of an ideally placed B (A) layer; $\mathbf{R}_{AB}$ ($\mathbf{R}_{BA}$) is the stacking height along the stacking direction for positioning a B (A) layer with respect to the previous A (B) layer; $\mathbf{u}$ is a reciprocal lattice vector ($\mathbf{u} = h\boldsymbol{a}^* + k\boldsymbol{b}^* + l\boldsymbol{c}^*$). The structure factor contribution, F_0, is a weighted sum of contributions from A or B layers:

$$F_0 = g_A F_A + g_B F_B \qquad [2]$$

F_1 contains an allowance for either a faulted or an unfaulted second layer and includes terms that incorporate the conditional probability that the first layer was A or B:

$$F_1 = g_A[(1 - \alpha_{AB}) + \alpha_{AB} \cdot \exp(2\pi i \mathbf{u} \cdot \mathbf{r}_{AB})]F_B \cdot \exp(2\pi i \mathbf{u} \cdot \mathbf{R}_{AB}) + g_B[(1 - \alpha_{BA}) + \alpha_{BA} \cdot \exp(2\pi i \mathbf{u} \cdot \mathbf{r}_{BA})]F_A \cdot \exp(2\pi i \mathbf{u} \cdot \mathbf{R}_{BA}) \qquad [3]$$

Thus, the first term accounts for the case where layer B stacks after A (which is present with probability g_A), and the second term accounts for the case where layer A stacks over layer B (which is present with probability g_B). Within each of these two terms are two parts, contributions for stacking without a fault and with faulting (with shifting vector $\mathbf{r}_{AB}$ or $\mathbf{r}_{BA}$). There is an allowance for a phase shift in this structure factor contribution due to the shifting vector $\mathbf{R}_{AB}$ or $\mathbf{R}_{BA}$ along the c direction. The contributions to F_2 can be dissected in a similar way:

$$F_2 = g_A[(1 - \alpha_{AB})\{(1 - \alpha_{BA}) + \alpha_{BA} \cdot \exp(2\pi i \mathbf{u} \cdot \mathbf{r}_{BA})\} + \alpha_{AB}\{(1 - \alpha_{BA}) + \alpha_{BA} \cdot \exp(2\pi i \mathbf{u} \cdot \mathbf{r}_{BA})\}$$

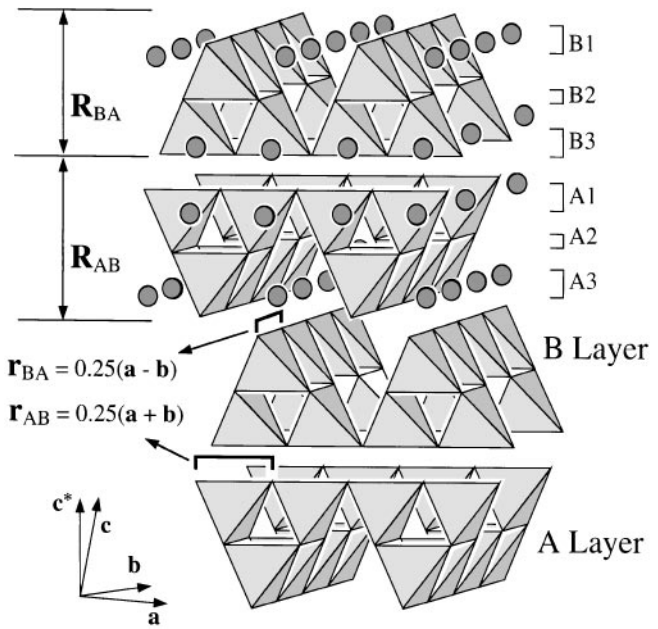

FIG. 5. Polyhedral presentation of the structure of KMQ_2 (M = Al, Ga; Q = Se, Te). The relationships of the faulting vectors, $0.25(\mathbf{a} - \mathbf{b})$ or $0.25(\mathbf{a} + \mathbf{b})$, are illustrated. For clarity, potassium cations are shown only in the two top layers.

$$\cdot \exp(2\pi i\mathbf{u}\cdot\mathbf{r}_{AB})]F_A \cdot \exp\{2\pi i\mathbf{u}\cdot(\mathbf{R}_{AB} + \mathbf{R}_{BA})\} + g_B[\cdots]$$

$$= g_A[(1-\alpha_{AB})(1-\alpha_{BA}) + (1-\alpha_{AB})\alpha_{BA} \cdot \exp(2\pi i\mathbf{u}\cdot\mathbf{r}_{BA}) + \alpha_{AB}(1-\alpha_{BA})\cdot\exp(2\pi i\mathbf{u}\cdot\mathbf{r}_{AB}) + \alpha_{AB}\alpha_{BA}\cdot\exp(2\pi i\mathbf{u}\cdot(\mathbf{r}_{AB}+\mathbf{r}_{BA})]F_A \cdot\exp\{2\pi i\mathbf{u}\cdot(\mathbf{R}_{AB}+\mathbf{R}_{BA})\} + g_B[\cdots]. \quad [4]$$

F_3, F_4, and $\cdots F_N$ are obtained in an analogous fashion. The total structure factor (F_T) is the sum of the F_i terms, which can be gathered and like rearranged to read

$$\begin{aligned}F_T = {} & g_A[F_A + (1-\alpha_{AB})F_B\cdot\exp(2\pi i\mathbf{u}\cdot\mathbf{R}_{AB}) \\ & + (1-\alpha_{AB})(1-\alpha_{BA})F_A\cdot\exp\{2\pi i\mathbf{u}\cdot(\mathbf{R}_{AB}+\mathbf{R}_{BA})\} \\ & + (1-\alpha_{AB})^2(1-\alpha_{BA})F_B\cdot\exp\{2\pi i\mathbf{u}\cdot(2\mathbf{R}_{AB}+\mathbf{R}_{BA})\} \\ & + \cdots + \alpha_{AB}\cdot\exp(2\pi i\mathbf{u}\cdot\mathbf{r}_{AB})\cdot\exp(2\pi i\mathbf{u}\cdot\mathbf{R}_{AB}) \\ & \times[F_B + (1-\alpha_{BA})F_A\cdot\exp(2\pi i\mathbf{u}\cdot\mathbf{R}_{BA}) \\ & + (1-\alpha_{BA})(1-\alpha_{AB})F_B\cdot\exp\{2\pi i\mathbf{u}\cdot(\mathbf{R}_{BA}+\mathbf{R}_{AB})\} \\ & + (1-\alpha_{BA})^2(1-\alpha_{AB})F_A\cdot\exp\{2\pi i\mathbf{u}\cdot(2\mathbf{R}_{BA}+\mathbf{R}_{AB})\} \\ & + \cdots + \alpha_{BA}\cdot\exp(2\pi i\mathbf{u}\cdot\mathbf{r}_{BA})\cdot\exp(2\pi i\mathbf{u}\cdot\mathbf{R}_{BA}) \\ & \times[F_A + (1-\alpha_{AB})F_B\cdot\exp(2\pi i\mathbf{u}\cdot\mathbf{R}_{AB}) \\ & + (1-\alpha_{AB})(1-\alpha_{BA})F_A\cdot\exp\{2\pi i\mathbf{u}\cdot(\mathbf{R}_{AB}+\mathbf{R}_{BA})\} \\ & + (1-\alpha_{AB})^2(1-\alpha_{BA})F_B\cdot\exp\{2\pi i\mathbf{u}\cdot(2\mathbf{R}_{AB}+\mathbf{R}_{BA})\} \\ & + \cdots]]] + g_B[\cdots]. \end{aligned} \quad [5]$$

The development outlined to this point is fairly general, but the particulars of the $KGaTe_2$ structure put strong constraints on the nature of the stacking faults and parameters introduced in the preceding discussion. Because of the manner in which adjacent A and B layers interdigitate, the layers can shift only in the $(\mathbf{a} - \mathbf{b})$ or $(\mathbf{a} + \mathbf{b})$ directions. Figure 5 illustrates this point. If we focus on the individual atoms within a layer, these constraints become even more restrictive. The stacking fault must introduce a minimal increase of the system's internal energy, so when a fault occurs the atoms external to each layer (the Te atoms) must it together in a way that is nearly identical to the manner in which they fit in the ideal (lowest energy) structure. With that in mind, one concludes that the allowable shifts are discrete, $\pm 0.25(\mathbf{a} + \mathbf{b})$ or $\pm 0.25(\mathbf{a} - \mathbf{b})$. Note that shifts $0.25(\mathbf{a} \pm \mathbf{b})$ and $-0.25(\mathbf{a} \pm \mathbf{b})$ are equivalent due to the C-centered symmetry that applies in this case.

Both layers A and B consist of three sublayers. In Figs. 5 and 6, these are labeled A1 and B1 (K (top), Te (top), and Ga (top)), A2 and B2 (Te (middle)), and A3 and B3 (K (bottom), Te (bottom), and Ga (bottom)). A shift of layer A by the fault vector $0.25(\mathbf{a} - \mathbf{b})$ results in a shift of sublayer A1 by $0.5\mathbf{a}$(or $0.5\mathbf{b}$ since the lattice is C-centered and $0.5\mathbf{a}$ and $0.5\mathbf{b}$ are equivalent) without an apparent shift of A2 and A3—to the extent that the $GaTe_4$ tetrahedra are not regular, this is not strictly true. A shift in layer A by $0.25(\mathbf{a} + \mathbf{b})$ shifts sublayer A3 only by $0.5\mathbf{a}$. A shift in layer B by $0.25(\mathbf{a} + \mathbf{b})$ shifts sublayer B1 only by $0.5\mathbf{a}$. A shift in layer B by $0.25(\mathbf{a} - \mathbf{b})$ gives rise to the shifting of sublayer B3 only by $0.5\mathbf{a}$. Faults never cause a shift in sublayers A2 and B2 because they consist of complete Te square nets in the *ab* plane, and shifting vectors are equal to the distance between the Te atoms in the square nets. Applying these constraints in Eqs. [2], [3], and [4], the structure factor of terms can be written as follows:

$$F_0 = g_A(F_{A1} + F_{A2} + F_{A3}) + g_B(F_{B1} + F_{B2} + F_{B3}) \quad [6]$$

$$F_1 = g_A[\{(1-\alpha_{AB}) + \alpha_{AB}\cdot\exp(2\pi i\mathbf{u}\cdot\mathbf{r}_{AB})\}F_{B1} + F_{B2} + F_{B3}]\cdot\exp(2\pi i\mathbf{u}\cdot\mathbf{R}_{AB}) + g_B[\{(1-\alpha_{BA}) + \alpha_{BA}\cdot\exp(2\pi i\mathbf{u}\cdot\mathbf{r}_{BA})\}F_{A1} + F_{A2} + F_{A3}]\cdot\exp(2\pi i\mathbf{u}\cdot\mathbf{R}_{BA}) \quad [7]$$

$$F_2 = g_A[\{(1-\alpha_{BA}) + \alpha_{BA}\cdot\exp(2\pi i\mathbf{u}\cdot\mathbf{r}_{BA})\}F_{A1} + F_{A2} + \{(1-\alpha_{AB}) + \alpha_{AB}\cdot\exp(2\pi i\mathbf{u}\cdot\mathbf{r}_{AB})\}F_{A3}] \cdot\exp\{2\pi i\mathbf{u}\cdot(\mathbf{R}_{AB}+\mathbf{R}_{BA})\} + g_B[\cdots] \quad [8]$$

$$F_3 = g_A[\{(1-\alpha_{AB}) + \alpha_{AB}\cdot\exp(2\pi i\mathbf{u}\cdot\mathbf{r}_{AB})\}^2 F_{B1} + F_{B2} + \{(1-\alpha_{BA}) + \alpha_{BA}\cdot\exp(2\pi i\mathbf{u}\cdot\mathbf{r}_{BA})\}F_{B3}] \cdot\exp\{2\pi i\mathbf{u}\cdot(2\mathbf{R}_{AB} + \mathbf{R}_{BA})\} + g_B[\cdots] \quad [9]$$

So, the total structure factor, F_T, is

$$\begin{aligned} F_T &= F_0 + F_1 + F_2 + F_3 + F_4 + \cdots + F_N \\ &= (F_0 + F_2 + F_4 + \cdots) + (F_1 + F_3 + F_5 + \cdots) \\ &= g_A\left[\frac{F_{A1} + F_{B3}\cdot\exp(2\pi i\mathbf{u}\cdot\mathbf{R}_{AB})}{1 - \{(1-\alpha_{BA}) + \alpha_{BA}\exp(2\pi i\mathbf{u}\cdot\mathbf{r}_{BA})\}\cdot\exp\{2\pi i\mathbf{u}\cdot(\mathbf{R}_{AB} + \mathbf{R}_{BA})\}} + 0.5N(F_{A2} + F_{B2})\right. \\ &\quad \left. + \frac{F_{A3} + F_{B1}\{(1-\alpha_{AB}) + \alpha_{AB}\cdot\exp(2\pi i\mathbf{u}\cdot\mathbf{r}_{AB})\}\cdot\exp(2\pi i\mathbf{u}\cdot\mathbf{R}_{AB})}{1 - \{(1-\alpha_{AB}) + \alpha_{AB}\exp(2\pi i\mathbf{u}\cdot\mathbf{r}_{AB})\}\cdot\exp\{2\pi i\mathbf{u}\cdot(\mathbf{R}_{AB} + \mathbf{R}_{BA})\}}\right] \\ &\quad + g_B\left[\frac{F_{B3} + F_{A1}\{(1-\alpha_{BA}) + \alpha_{BA}\cdot\exp(2\pi i\mathbf{u}\cdot\mathbf{r}_{AB})\}\cdot\exp(2\pi i\mathbf{u}\cdot\mathbf{R}_{BA})}{1 - \{(1-\alpha_{BA}) + \alpha_{BA}\exp(2\pi i\mathbf{u}\cdot\mathbf{r}_{BA})\}\cdot\exp\{2\pi i\mathbf{u}\cdot(\mathbf{R}_{AB} + \mathbf{R}_{BA})\}} + 0.5N(F_{A2} + F_{B2})\right. \\ &\quad \left. + \frac{F_{B1} + F_{A3}\cdot\exp(2\pi i\mathbf{u}\cdot\mathbf{R}_{BA})}{1 - \{(1-\alpha_{AB}) + \alpha_{AB}\exp(2\pi i\mathbf{u}\cdot\mathbf{r}_{AB})\}\cdot\exp\{2\pi i\mathbf{u}\cdot(\mathbf{R}_{AB} + \mathbf{R}_{BA})\}}\right]. \end{aligned} \quad [10]$$

From the symmetry of layers, we can reasonably assume that $g_A = g_B = 0.5$, $\alpha_{AB} = \alpha_{BA} = \alpha$, $\mathbf{r}_{AB} = \mathbf{r}_{BA} = 0.5\mathbf{a}$ (or $0.5\mathbf{b}$), and $\mathbf{R}_{AB} = \mathbf{R}_{BA} = \boldsymbol{c}' = \boldsymbol{c}/2$. Then $F_T(hkl)$ reduces to

$$F_T(hkl) = 0.5\left[\frac{(F_{A1} + F_{B1})\{2 - \alpha(1-(-1)^h)\} + 2(F_{A3} + F_{B3})}{\alpha(1-(-1)^h)} + N(F_{A2} + F_{B2})\right]. \quad [11]$$

We can see that $F_T(hkl) = 0.5N(F_{A1} + F_{A2} + F_{A3} + F_{B1} + F_{B2} + F_{B3}) = 0.5N(F_A + F_B)$ if $h = k = 2n$, from Eqs. [6]–[9], which is equal to the structure factor without faulting ($\alpha = 0$). However, the magnitude of the total structure factor, F_T, in Eq. [11] is reduced when h and k are odd (and will depend on α) because of destructive interference of diffraction intensities between sublayers. Intensities at the reciprocal points for half of the data set ($2h + 1$, $2k + 1$, l) should be reduced, and background intensities between the reciprocal points should be increased significantly, to an extent that depends on the fault frequency α. This explains why streaks and diffuse reflections are observed in half of the data set ($2h + 1$, $2k + 1$, l), and the other half is intact.

It is likely that the degree of planar faulting (α) is different from crystal to crystal, as qualitatively indicated by differences we observe in streaks and diffuse reflections in

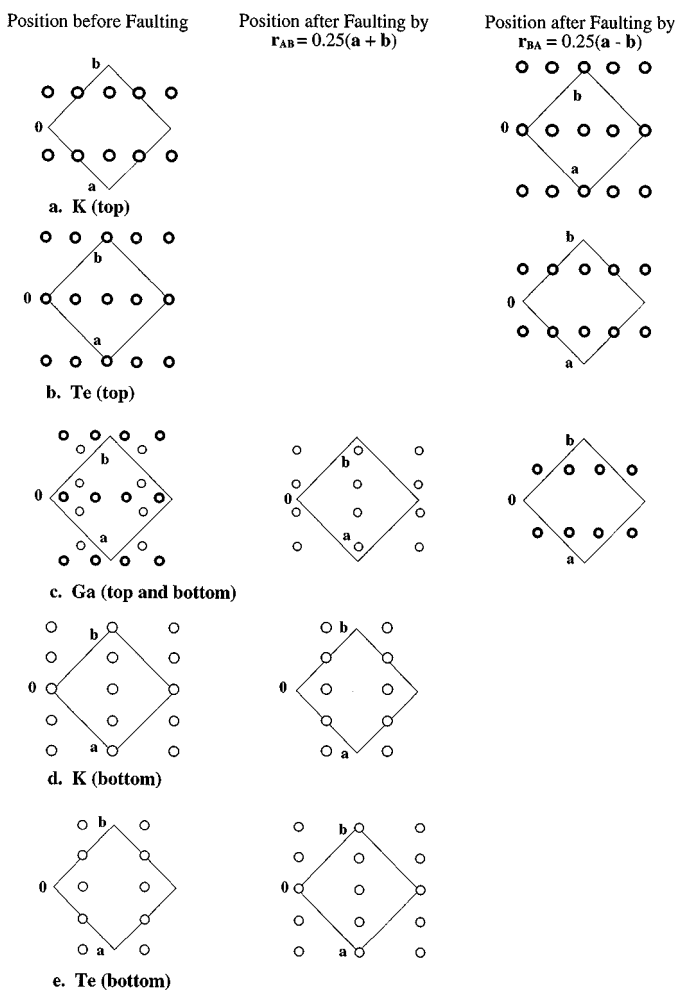

FIG. 6. Arrangements of each component in Layer A projected down the c^* axis before and after translation by faulting vectors. Only atoms whose positions are changed are shown. Layer A consists of three sublayers labeled A1 (K (top, a), Te (top, b), and Ga (top, c)), A2 (Te (middle)), and A3 (K (bottom, d), Te (bottom, e), and Ga (bottom, c)). Inspection of all these diagrams reveals that the net shift of the atomic positions is $0.5\mathbf{a}$ or $0.5\mathbf{b}$. Sublayer A2 is not shifted by either faulting vector.

rotational photographs. Planar faulting is presumably responsible for the triclinic cell (close to tetragonal cell) parameters reported by earlier investigators for compounds with this structure type, AMQ_2 (A = K, Tl; M = Al, Ga; Q = S, Se, Te) (21,37,38). Diffuse reflections and streaks give rise to the ambiguities in the determination of cell parameters and difficulties in the data collection processes for this type of compound. Pseudo-tetragonal cell parameters can be understood as derived from the two-dimensional tetragonal arrangement of atoms obtained when the structure is projected onto the *ab* plane.

We have used the DIFFaX program to calculate diffraction intensities for $KGaTe_2$ with varying faulting probabilities ($\alpha = 0.0, 0.1, 0.2, 0.5$). Atomic coordinates of the input file for DIFFaX program were generated by applications of faulting vectors, $0.25(\mathbf{a} - \mathbf{b})$ and $0.25(\mathbf{a} + \mathbf{b})$, to the coordinates of the ordered structure of $KGaTe_2$. The detailed procedures for the generation of output files of selected area diffraction patterns (*sadp*) are described in Section 3.7.4 (p. 30) in the DIFFaX program manual (27). The binary output file (extension name is *sadp*) was converted to a real image (256×256 pixel size) by use of the NIH Image program (version 1.6). The results are shown in Fig. 7 for reflections in the $h = k$ plane. As described in the analytical discussion above, reflection sets ($2h + 1$, $2k + 1$, l; $h = k$) become streaks as α increases, but ($0kl$) and ($h0l$) data are not changed. This is entirely consistent with observed oscillation photographs (see Fig. 1).

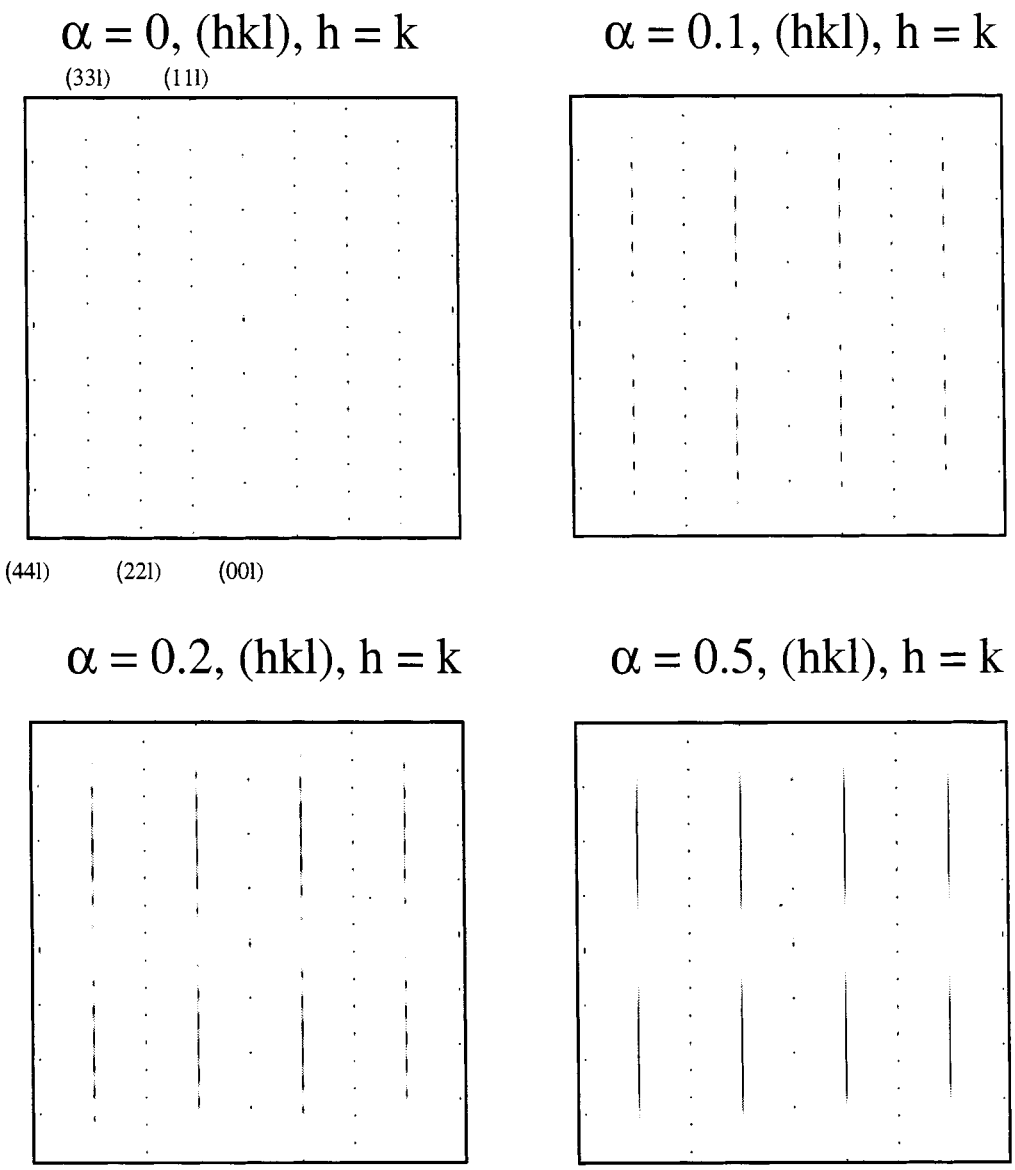

FIG. 7. Simulated reflection patterns of the $h = k$ plane for $KGaTe_2$ by changing faulting probability α.

CONCLUSIONS

The layered compounds KMQ_2 (M = Al, Ga; Q = Se, Te) have been prepared and characterized by the use of single-crystal X-ray studies, microprobe analyses, and atomic absorption measurements. These compounds are order–disorder type compounds with planar faults manifested by diffuse reflections and streaking along c^* directions. Two geometrically and energetically competitive interlayer stacking possibilities are responsible for the planar faults. Analytical structure factor calculations based on the modified summed series formula show that only half of the data set is affected by this type of faulting, a result that is entirely consistent with both the observed reflection data set and the simulated diffraction patterns obtained with the DIFFaX program.

ACKNOWLEDGMENTS

This research was generously supported by the Texas Advanced Research Program through Grant 010366-0038b. The R3m/V single-crystal X-ray diffractometer and crystallographic computing system were purchased from funds provided by the National Science Foundation (Grant CHE-8513273). We thank Dr. Renald Guillemette and Dr. Anatoly Bortun for their assistance with the microprobe analyses and atomic absorption measurements. We also thank Dr. M. Treacy (NEC Research Center, NJ) for providing the DIFFaX manual and for his valuable advice in performing computer simulations. Private communications with Dr. S. T. Hong (Department of Chemistry, Iowa State University) and Dr. Patrick Woodward (Department of Chemistry, Ohio State University) were crucial in the untangling of our investigations.

REFERENCES

1. M. M. J. Treacy, J. M. Newsam, and M. W. Deem, *Proc. R. Soc. London* **A433,** 499–520 (1991).
2. K. Dornberger-Schiff and H. Grell-Niemann, *Acta Crystallogr.* **14,** 167–177 (1961).
3. K. Dornberger-Schiff, *Acta Crystallogr.* **9,** 593–601 (1956).
4. V. H. Jagodzinsky, *Acta Crystallogr.* **7,** 17–25 (1954).
5. R. G. Hazell and S. Jagner, *Acta Crystallogr.* **B31,** 1412–1416 (1975).
6. V. H. Jagodzinsky, *Acta Crystallogr.* **2,** 201–207 (1949).
7. J. M. Cowley, *Acta Crystallogr.* **A32,** 83–87 (1976).
8. J. M. Cowley, *Acta Crystallogr.* **A32,** 88–91 (1976).
9. J. M. Cowley and A. Y. Au, *Acta Crystallogr.* **A34,** 738–743 (1978).
10. E. Michalski, *Acta Crystallogr.* **A44,** 640–649 (1988).
11. E. Michalski, *Acta Crystallogr.* **A44,** 650–657 (1988).
12. J. D. Dunitz, "X-Ray Analysis and the Structure of Organic Molecules." Cornell University Press, Ithaca, NY, 1979.
13. D. Schwarzenbach, *Z. Kristallogr.* **128,** 97–114 (1969).
14. S. Hendricks and E. Teller, *J. Chem. Phys.* **10,** 147–167 (1942).
15. A. J. C. Wilson, *Proc. R. Soc. London* **A180,** 277–275 (1942).
16. A. J. C. Wilson, *Proc. R. Soc. London* **A181,** 360–368 (1943).
17. J. Kim, C. Wang, and T. Hughbanks, *Inorg. Chem.* **37,** 1428–1429 (1998).
18. J. Kim, C. Wang, and T. Hughbanks, *Inorg. Chem.* **38,** 235–242 (1999).
19. J. Kim and T. Hughbanks, *J. Solid State Chem.* **146,** 217–225 (1999).
20. C. Wang, J. Kim, and T. Hughbanks, *in* "Materials Research Society Symposium Proceedings" (A. Jacobson, P. Davies, T. Vanderah, and C. Torardi, Eds.), pp. 23–28. Materials Research Society, Boston, MA, 1997.
21. J. Weiss, H. Schäfer, and G. Schön, *Z. Naturforsch* **31b,** 1336–1340 (1976).
22. B. Eisenmann and A. Hofmann, *Z. Kristallogr.* **197,** 145–146 (1991).
23. B. Eisenmann and A. Hofmann, *Z. Kristallogr.* **197,** 153–154 (1991).
24. B. Eisenmann and A. Hofmann, *Z. Kristallogr.* **197,** 157–158 (1991).
25. B. Eisenmann and A. Hofmann, *Z. Kristallogr.* **197,** 173–174 (1991).
26. B. Eisenmann and A. Hofmann, *Z. Kristallogr.* **197,** 163–164 (1991).
27. M. M. J. Treacy, M. W. Deem, and J. M. Newsam, DIFFaX Program v1.801, 1995. [Program manual was generously provided by Dr. M. M. J. Treacy.]
28. F. Feher, *in* "Handbuch der Präparativen Anorganischen Chemie" (G. Brauer, Ed.). Ferdinand Enke Verlag, Stuttgart, Germany, 1954.
29. W. Klemm, H. Sodomann, and P. Langmesser, *Z. Anorg. Allg. Chem.* **241,** 281–304 (1939).
30. O. Conrad, A. Schiemann, and B. Krebs, *Z. Anorg. Allg. Chem.* **623,** 1006–1010 (1997).
31. V. A. Schneider and G. Gattow, *Z. Anorg. Allg. Chem.* **277,** 49–59 (1954).
32. K. Range and H. Hübner, *Z. Naturforsch* **28b,** 353–355 (1973).
33. G. A. Steigmann and J. Goodyear, *Acta Crystallogr.* **20,** 617–619 (1966).
34. J. L. Pouchou and F. Pichoir, *La Recherche Aerospatiale* **3,** 13–38 (1984).
35. G. M. Sheldrick, "SHELXTL-93 User Guide." Crystallography Department, University of Göttingen, Germany, 1993.
36. V. D. Müller and H. Hahn, *Z. Anorg. Allg. Chem.* **438,** 258–272 (1978).
37. H. Hahn and B. Wellmann, *Naturwissenschaften* **54,** 42–42 (1967).
38. F. E. Poltmann and H. Hahn, *Naturwissenschaften* **58,** 53–54 (1971).